Progress In Electromagnetics Research, PIER 101, 43–62, 2010

THE EXPERIMENTAL RESULTS OF A LOW POWER X-BAND FREE ELECTRON MASER BY ELECTRON PRE-BUNCHING

F. Malek

School of Computer and Communication Engineering
Universiti Malaysia Perlis (UniMAP)
No. 12 & 14, Jalan Satu, Taman Seberang Jaya Fasa 3, Kuala Perlis 02000, Perlis, Malaysia

J. Lucas and Y. Huang

Department of Electrical Engineering and Electronics
The University of Liverpool
Brownlow Hill, Liverpool L69 3GJ, United Kingdom

Abstract—We have developed a proof-of-concept low power free electron maser that is compact and low cost. The design, set-up and results of a novel (without wiggler) low power X-band rectangular waveguide pre-bunched free electron maser (PFEM) are presented in this paper. Our device operates at 10 GHz, with 10 mWatt seeding input power and employs two rectangular waveguide cavities (one for velocity modulation and the other for energy extraction). The electron beam used in this experiment is produced by Thoria coated Iridium filament which can operate at 3 kV and up to 5 mA beam current. The effect of the aperture on the power leaking out of the waveguide is also analyzed. The TE_{10} mode propagation of the EM standing wave is used to pre-bunch the electron beams in the input cavity. The bunched electron beams are in the same phase as the TE_{10} mode propagation of the EM wave in the output cavity. This free electron maser could be useful industrially, as it could be used with the commercially available accelerating voltage supplies.

Corresponding author: F. Malek (mfareq@unimap.edu.my).

1. INTRODUCTION

The free electron maser (FEM) is a source of microwave power which makes use of the interaction between the electron beam and electromagnetic radiation [1, 2]. In a uniform electron beam, the contributions of individual electrons to the random field are random in phase. Hence, the square of the total field is equal to the sum of the squares of the individual fields. If the electrons are bunched within a distance comparable to the wavelength of the radiation, their fields would add up in phase, resulting in coherent emission radiation. The power level of the coherent radiation generated by a bunched electron beam is typically several orders of magnitude higher than the non-coherent radiation generated by a uniform electron beam. Motz has proposed the idea of generating coherent radiation by utilizing bunched electron beams [3]. Sirkis has investigated the different methods of coupling structure, used to extract the energy at a harmonic of the bunch repetition rate [4]. Pantel has discussed the problem of synchronism between the propagation of the wave and the electron beam motion [5].

In any FEL system, to have a sustained interaction, the electron and electromagnetic wave have to travel in phase. The electron must travel at a speed approximately equal to the phase velocity of the EM wave to enable a sustained interaction. This cannot be achieved since the electron velocity is always less than the velocity of light, c, and the phase velocity of the EM wave is always greater than c in a free space waveguide. This difference in speed means that the electron would slip in phase with respect to the wave and average energy exchange will be zero.

In the dispersion curve (ω-β diagram) of a wiggler FEL system, the λ_w (lambda wiggler) value could be altered so that the dispersion curve of the EM wave in the waveguide can intersect the electron beam line [6, 7]. In the wiggler FEL system, the initial path of the electrons is in the same direction as the path of the injected EM wave in the rectangular waveguide. The aim is for these electrons to interact with the TE_{10} mode direction of the EM wave.

As the electron travels along the z-axis it experiences a magnetic field due to the alternating polarity magnetic bars. Under the influence of this field, an electron traveling along the z-axis experiences a force which causes it to oscillate in the x-z plane. Hence, the wiggler provides the electron with a transverse component of velocity, allowing it to couple to the transverse electric field of the EM wave. The diagram of the wiggler FEL is shown in Figure 1.

In the wiggler FEL system, the initial path of the electrons is in

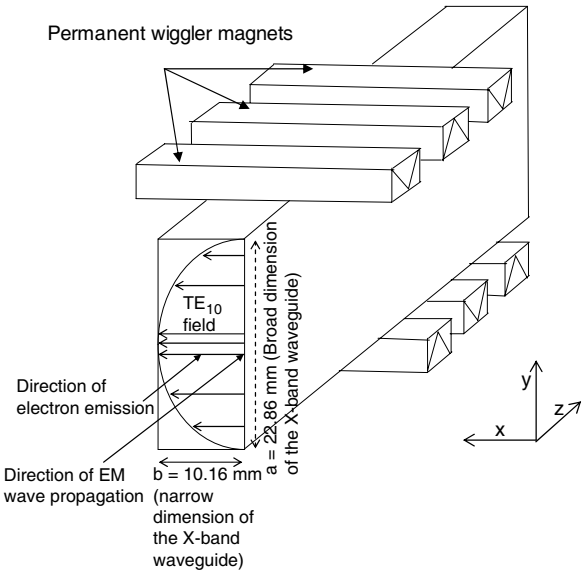

Figure 1. Diagram of the wiggler FEL, showing the directions of initial electron emission and EM wave propagation.

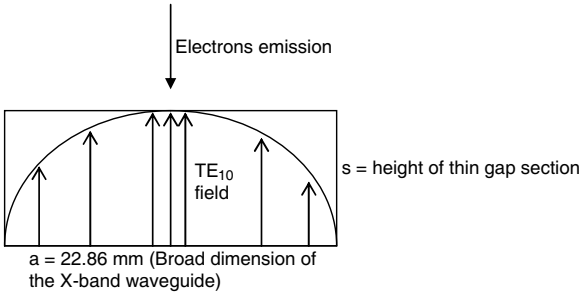

Figure 2. Direction of electron emission in PFEM waveguide.

the same direction as the path of EM wave. In order for the electrons to interact with the TE_{10} mode direction of the EM wave, the wiggler is used. In other words, the electron beam line is now intersecting the EM wave curve in the dispersion diagram, by using the correct wiggler parameters [8]. In the low power PFEM system, the path of the electrons is not in the same direction as the path of the injected EM wave. In this PFEM system, the electron is emitted in parallel with the TE_{10} direction of the EM wave, as can be seen in Figure 2.

In the PFEM system, the electron beams interact with the EM

wave by having them emitted in the same direction (parallel) with the TE_{10} mode direction of the EM wave. The important factor for the PFEM operation is the transit time of electrons in the thin gap section of the waveguide. This is to ensure that the interaction between the electrons and EM wave occurs at the correct phase of the EM wave. The thin gap section makes a short electron transit time possible and increases the intensity of the electric field through which the electron passes [9–11]. The height of the thin gap section is designed, such that the transit time of electrons in the thin gap section is less than the time for half of a wavelength of the standing wave sinusoidal waveform [12]. The transit time of the electrons in the thin gap section has been described in [1].

Low voltage free electron masers are of considerable interest both theoretically and practically. For instance, they can be designed so that the electron beam interacts with the dominant TE mode only rather than much more complex interaction which occurs in higher voltage types employing overmoded free electron laser waveguides. Low voltage waveguide FELs are also capable of higher efficiency than standard FELs [13]. This, added to the fact that with commercially available accelerating voltage supplies, continuous operation is possible, means that these devices could be useful industrially. In this small signal gain region, the effects of the space charge between the electrons are not taken into the design consideration. The free electron maser operating in the small signal gain region (low acceleration voltage and current) could be useful to avoid effects that might reduce the stability of the output.

We have developed a novel pre-bunched free electron maser (PFEM) operating at a relatively low voltage of 3 kV at a frequency of 10 GHz. The proof-of-concept system, shown in Figure 3 and Figure 4, consists of an input rectangular cavity (for velocity modulation of the electron beams) and an output rectangular cavity (for energy extraction). The initial experiment was performed with a beam current of up to 50 μA to check for suitability and feasibility [1]. In this paper, further experiments are undertaken, which demonstrate coherent emission and gain with a beam current up to 5 mA.

This novel design scheme (without wigglers) allows the PFEM to operate at a low current and accelerating voltage, maintaining a compact design. The acceleration voltage is applied directly between the electron gun filament and input cavity. The same X-band microwave source is fed into both the cavities. The phase between the output and the input cavities can be tuned by employing a phase shifter. The velocity modulated electron beam from the input cavity interacts with the microwave E-field in the output cavity, which emits

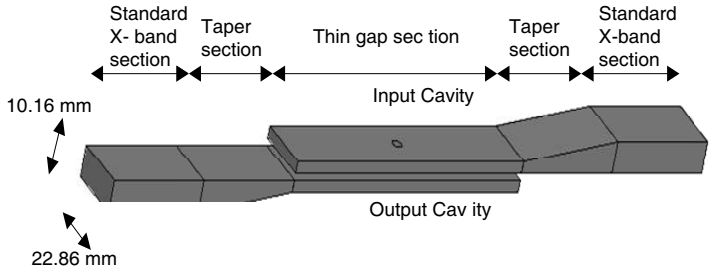

Figure 3. Diagram of the low power PFEM showing the input cavity and the output cavity.

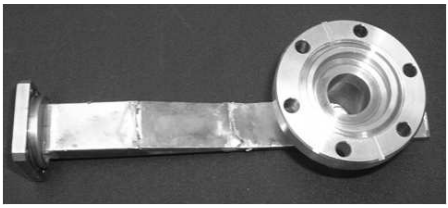

Figure 4. An actual low power PFEM cavity.

strong coherent radiation. As a result, enlarged microwave power can be obtained [13–15].

Most FEL research either operates at very high voltage or current, or both. In most cases, the FEL cost is very expensive. This research project is unique because the FEM uses low voltage and low current. Due to the low voltage, the output frequencies are in the microwave frequency range, where monitoring equipment is more readily available and cheaper. The equipment breakdowns are rare, and the ionizing (X-ray) radiation is not dangerous. Due to the low current, it is easy to maintain the high vacuum condition. Due to both (low voltage and low current), the PFEM system can be operated (powered) from the main socket (240 Volts and 13 A) [1].

The operating frequency of the PFEM can be tuned by simply adjusting the acceleration voltage. This means that the PFEM can be made at a cost cheaper than the currently available microwave source. The initial results have been presented in detail in [1]. The low power PFEM design concept, system implementation and mathematical analysis are explained in [1]. The photographs of the final components and system are illustrated in this paper. Figure 5 shows the photograph of the input cavity circuit, while Figure 6 shows the photograph of the output cavity circuit. The photograph of the

overall low power PFEM system is shown in Figure 7. The next sections analyze the power leaking out of the waveguide, the mesh constructed at the aperture of the output cavity and the final results of the low power PFEM device.

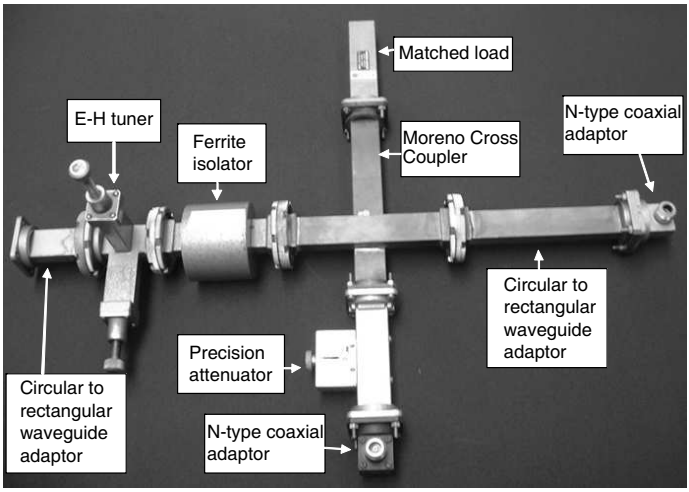

Figure 5. Photograph of the input cavity circuit.

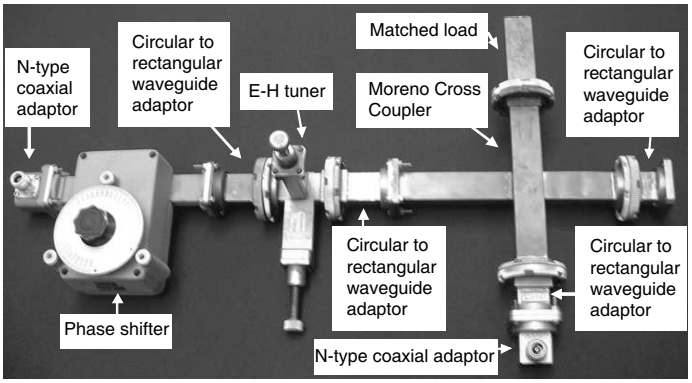

Figure 6. Photograph of the output cavity circuit.

2. THE APPLICATIONS OF THE FREE ELECTRON LASER

The potential applications of the free electron laser, as a tuneable power source in the X-band spectrum, are microwave plasma torch

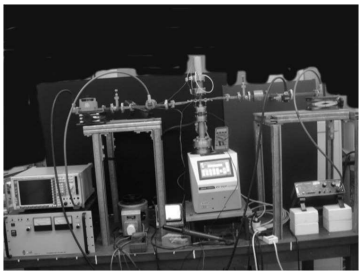

Figure 7. Photograph of the low power PFEM system.

and microwave driven plasma discharge. The applications of microwave plasma torch are for welding and cutting of metals and ceramics [16, 17]. The microwave-driven plasma discharge is used for breaking down toxic organic substances into their less harmless constituent elements for pollution control [16–18]. In both cases, the wavelength may be selected for optimum performance of the process.

The free electron laser may also be potentially used in the radar device, if the tunability could be implemented with high output power and efficiency. If the wavelength ranges from 3 mm to 300 μm, the free electron laser may be potentially applied as a variable wavelength source to optimize the increase in chemical reaction rates induced by the applications of microwaves [16, 17]. Applications for solid inorganic materials are transformation in hardening of metals, heating of glass and ceramics, melting of concrete and stress hardening of glass. Applications for solid organic materials are cooking, drying, paint and welding plastics. Applications for liquid materials are pasteurization and sterilization, glue softening, crystallization and casting processes [16–18]. The 30–300 μm wavelength stage is designed to study the same problems as the previous wavelength range but the shorter wavelength would be expected to have different penetration and absorption characteristics.

In addition to that, the free electron laser potential implementation in the THz spectrum (below 300 μm wavelength) would lead to the following benefits [16–18]:

(a) A tunable EM wave source for researching the wave interaction of materials.

(b) Enhancement of the industrial processes by THz plasma generation, fine chemical production, bio-engineering to use the EM wave to supply nutrients to promote cell growth and medical imaging to compliment X-ray imaging but without tissue damage.

(c) The military applications are for weapons and toxic gas detection.

The typical power requirements for the various mentioned applications are typically up to 6 kWatt. However, for the THz spectrum, there are currently only a few THz radiation sources available, and these can only produce low output beam powers (of the order of microwatts to milliwatts). These are listed in Table 1 and are based upon the current technologies of semiconductor electronics and optical technologies.

Table 1. The main devices in the THz spectrum.

Sources (Instruments)	Frequency (THz)	Power
Si-Impatt devices	0.4	2 mW at 77°K
RTD Resonant Tunneling Diodes	0.7	1 μW
GaAs Tunnett Diodes	0.2 (Second harmonic)	10 mW at 300°K
Schottky Multipliers (mm-wave sources)	0.4, 0.8, 1.2	12 mW,2 mW,0.2 mW
Heated powder films	60	100 μW
Quantum Cascade Laser	2–60	0.1 mW to 100 mW

Therefore, the free electron laser could be a potential technology to bridge this current THz gap. The proof-of-concept PFEM device could be further developed that would lead to suitability for industrial applications. Compared with other lasers, the FEL has two significant advantages: they are readily tunable within a very wide frequency range and can be potentially engineered to very high power with relatively straightforward engineering. Due to its technical superiority, the FEL should be able to compete successfully in equal terms with lasers. The suitability of FEL also depends on whether the FEL is cost effective compared to lasers or other energy sources. The engineering of low cost, compact and high efficiency free electron laser is an important aspect of research at Universiti Malaysia Perlis and The University of Liverpool.

3. THE POWER LEAKING OUT OF THE WAVEGUIDE

The effect of the E-field pattern on the power leaking out from the waveguide into the tunnels is investigated by using the electromagnetic software package Vector Fields CONCERTO. The effect on the E-field pattern is observed for an aperture diameter of 1.5 mm with the height of the thin gap section of 1.5 mm. In CONCERTO software, the default medium in the drawing window is perfect electrical conductor (PEC). In order to design the required PFEM, each component of the waveguide is filled with air, i.e., the waveguide is "hollowed out" metal.

With CONCERTO software, it is possible to simulate the structure with apertures on either side of the wall of the structure. To simulate apertures drilled across the height of the thin gap section, a cylinder is drilled across this height. However, since the spaces above and at the bottom of this thin gap section are PEC, there are reflections of electric fields back into the cylinder and the waveguide due to this PEC. If this happens, the result of the electric field pattern near the apertures is not accurate. To overcome this problem, the cylinder is extended on each side of the wall of the waveguide, as shown in Figure 8. This extended cylinder also allows the simulation of the effect of the electric field leaking out from the waveguide.

An 8 mm length cylinder with 1.5 mm radius causes a high attenuation, and the resultant E-field is only approximately $3.18 \times 10^{-7}\%$ of the initial amplitude. This means that only a small strength E-field are present at the 8 mm point of the cylinder (bordering the PEC) and are reflected back to the cylinder from the wall of the PEC. This small reflection does not affect the larger E-field leakage near the aperture. Therefore, an 8 mm cylinder length is sufficient to be used in CONCERTO to simulate the leakage radiation caused by the apertures in the thin gap section.

The envelope plot of the E-field strength in the X direction is shown in Figure 9 where the effect of a 1.5 mm diameter aperture can be seen to reduce the E-field strength at the centre of the peak amplitude in the thin gap section. The TE_{10} mode propagation of the wave as seen in Figure 10 also shows a reduction of E-field at the centre of the broad wall of the waveguide. The 3-D propagation of the wave in Figure 11 shows this reduction of E-field strength on the centre peak amplitude. The accelerating E-field experienced by an electron crossing a waveguide section in the X direction is no longer the ideal 'top hat' rectangular function of position, but smeared out [21, 22]. The E-field pattern and leakages at the apertures for three different scenarios are simulated. The three scenarios and the percentage of the E-field leakage due to the aperture are shown in Table 2.

Table 2. The percentage of the E-field leakage for various aperture diameters and heights of the thin gap sections.

Height of the thin gap section (mm)	Aperture diameter (mm)	The percentage of the E-field leakage (%)
1.5	3.0	56.8
1.5	1.5	27.9
1.5	0.75	22.8

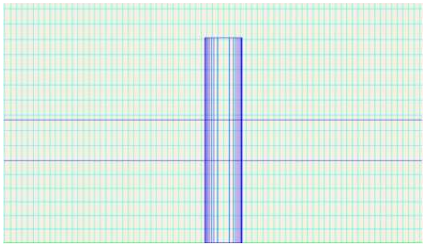

Figure 8. A cylinder going through the waveguide, to simulate the apertures in CONCERTO software.

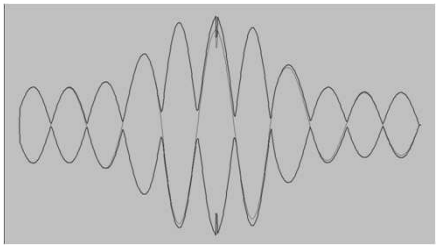

Figure 9. The envelope plot in the X direction, where the effect of the aperture on the peak E-field amplitude is shown.

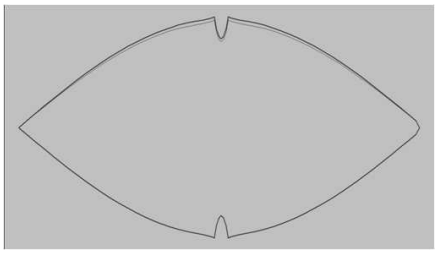

Figure 10. The envelope plot of the wave in the Z direction.

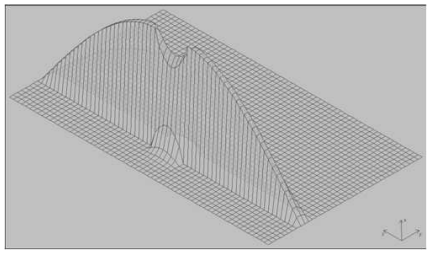

Figure 11. The TE_{10} mode plot viewed on the YZ plane at the middle of the x-axis for the case of apertures present on the waveguide, for the case of 1.5 mm central width and 1.5 mm of aperture diameter.

As can be expected, as the aperture diameter becomes smaller, the E-field leakage becomes smaller too. The aperture diameter of 1.5 mm and a 1.5 mm height of thin gap section are chosen as the PFEM design dimensions. Although the E-field leakage for the 0.75 mm aperture diameter is smaller than that for the 1.5 mm diameter aperture, the construction of this 0.75 mm aperture diameter is more difficult and requires more precision.

4. A MESH CONSTRUCTED AT THE APERTURES OF THE OUTPUT CAVITY

Without a mesh, when a high voltage is applied between the filament and input cavity, a very small amount of electron beams flows across (only 10% of the total filament current). This is due to the electrons flowing to the edges of the aperture because the shorter distance traveled compared to the centre of the aperture.

There are two possible solutions to this problem. One solution is to place a mesh on the aperture, and the other is to increase the diameter of the aperture. Increasing the aperture diameter will cause the E-field of the EM wave not to be vertical (will be skewed at a certain angle). This will result in a weak E-field component when interacting with the incoming electron beam. Therefore, the solution chosen is to place a mesh on the aperture. This mesh is made of a stainless steel with 4 mm diameter, and is silver soldered on top of the aperture of the cavity, as shown in Figure 12.

The next issue is to decide in which cavity to place the mesh. The electrons will travel to the shortest distance from the filament tip. If the shortest distance is the mesh at the input cavity, then the electrons will travel in a straight line path to the mesh. After encountering this mesh, the next shortest distance will be the edges of the aperture at the output cavity. Therefore, the electrons will not flow across the apertures of the output cavity.

Hence, the solution is to place the mesh at the output cavity. In this way, the electrons will see the mesh as the shortest distance from the filament tip. Therefore, the electrons will flow in a straight line path from the filament tip to the mesh. In this way, the electrons are forced to travel into the apertures of the output cavity. The following arrangement in Figure 13 shows the set-up for the experiment.

The High Voltage (HV) power supply supplies the high voltage to

Table 3. The current flow across the apertures when a mesh is located on the aperture of the output cavity.

Volts	I_t (μA)	I_1 (μA)	I_4 (μA)
1000	50	25.0	25.0
1500	50	25.0	25.0
2000	50	25.0	25.0
2500	50	25.0	25.0
3000	50	25.0	25.0

the tungsten filament, while the filament transformer supplies a high current for the heating of the tungsten filament. It can be seen that the filament is set at a high voltage, while the input and output cavities are set at an earth potential. A 100 kΩ resistor is placed in between the high voltage line and tungsten filament for safety purposes. The 509 kΩ resistor consists of two 9.9 kΩ resistors and thirty three 17.9 kΩ resistors, cascaded in series. The filament transformer and copper tube attached to the thin gap sections of the input and output cavities

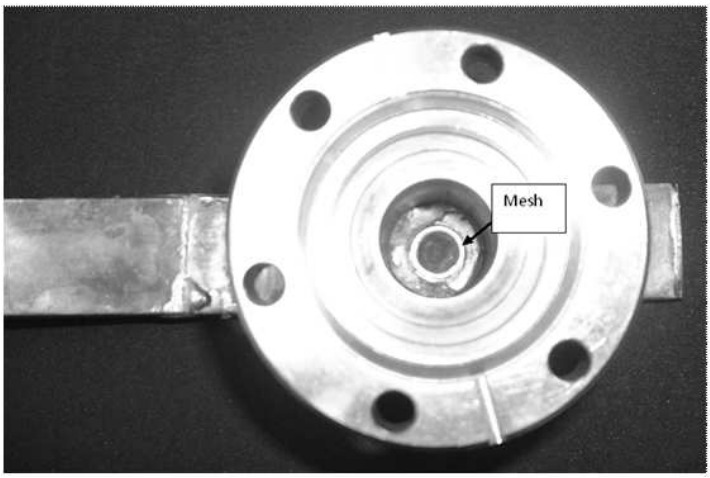

Figure 12. A mesh constructed on top of the aperture of the cavity.

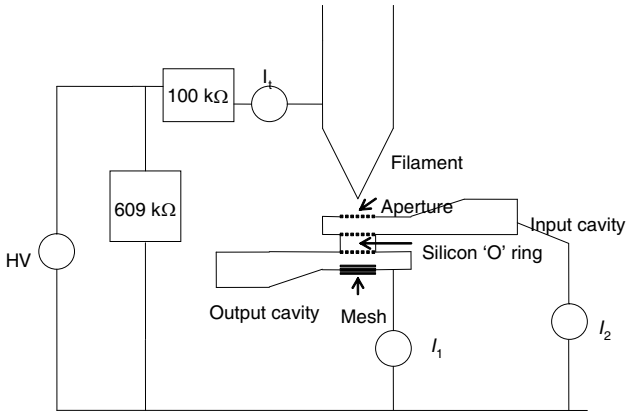

Figure 13. The circuit arrangement for measuring the current across the apertures with a mesh located on the aperture of the output cavity.

respectively have been omitted for diagram simplicity.

The two micro-ammeters are set-up as shown in Figure 13 to measure the current flowing from each cavity to the ground. The current flowing from the input cavity to ground is I_2, and the current flowing from the output cavity to ground is I_1. The high voltage is varied from 1000 to 3000 Volts, while the total filament current, I_t, is fixed to 50 μA. The results are shown in Table 3.

The above result shows that 50% of the total filament current flows across the aperture of the output cavity. This result is satisfactory since half of the bunched beam (50%) will now be able to interact with the EM wave in the output cavity. This figure (50%) is consistent with the result obtained from Dearden's experiment where he showed that a total beam transmission, from gun to collector, of 60% could be achieved [23].

It is desirable to have the filament to input cavity spacing at a minimum, since this would lead to less interception by the input cavity (depending on its aperture size) [24]. The distance between the tip of the filament and the input cavity aperture is 1 mm. If the filament is set too near or in the aperture, the emission current will be limited by space charge. This separation distance is found to be sufficient to allow reliable operation at 3 kV without breakdown. The input cavity aperture size of 1.5 mm in diameter provides a low input cavity loss and avoids excessive diverging of the beam.

5. RESULTS AND DISCUSSION

After achieving a satisfactory result for the current flow across the apertures of the output cavity, the next experiment could be performed. Thoria coated Iridium filament is used as the new electron beam source. The advantage of this Thoria coated iridium filament source is that it can produce a maximum current emission of 20 mA compared to the 200 μA produced by the tungsten filament source. A 10 mA total filament current is used because if 20 mA total filament current is used, the value of the perveance is 1.22×10^{-7}, which is larger than 10^{-8}. Hence space charge effect of the gun cannot be neglected. Moreover, at a total filament current higher than 10 mA, the pressure reading goes up very quickly from 10^{-8} mbar to 10^{-4} mbar due to outgassing, which shortens the lifetime of the filament dramatically.

An experiment has been set-up so that a voltage difference up to -3.2 kV occurs between the Thoria coated Iridium filament and input cavity. There is no voltage difference between the input and output cavities. The output cavity is placed directly below the input cavity, separated by silicon 'O' ring for insulation purpose [1]. This insulation

is to allow the current to flow through the apertures to be measured. In the vacuum system, the pump is isolated from the output cavity by a glass spacer, for the purpose of current measurement flowing across the apertures of the cavities.

The phase shifter is placed at the output cavity, where the phase of the output cavity in relation to the input cavity can be varied between 0 to 360 degrees. The filament current is set to 10 mA, and 10 GHz operating frequency is chosen. It is observed that 50% of this total filament current flows across the apertures of the output cavity. The term used for this is the beam current, and hence the beam currents used in the experiment is 5 mA. The output power level (dBm) reading is observed when the filament is cold. The reading is called the reference power level (dBm). The filament is heated up to the desired beam current (5 mA), and the output power level (dBm) is observed. This reading is called the observed power level (dBm). The gain is the difference between the observed power level (dBm) and the reference power level (dBm). The beam current (current across the apertures of the output cavity) recorded is 5 mA for 10 mA total filament current used, i.e., 50% of the total filament current.

The result of the variation in output cavity power with beam voltage is shown in Figure 14, for a seeding power of 10 mWatt. This plot can also be called the gain-voltage curve. For the above case, the beam current used is 5 mA. The voltages are varied in increments of 15 Volts, ranging from about 2700 up to 3200 Volts. The curve

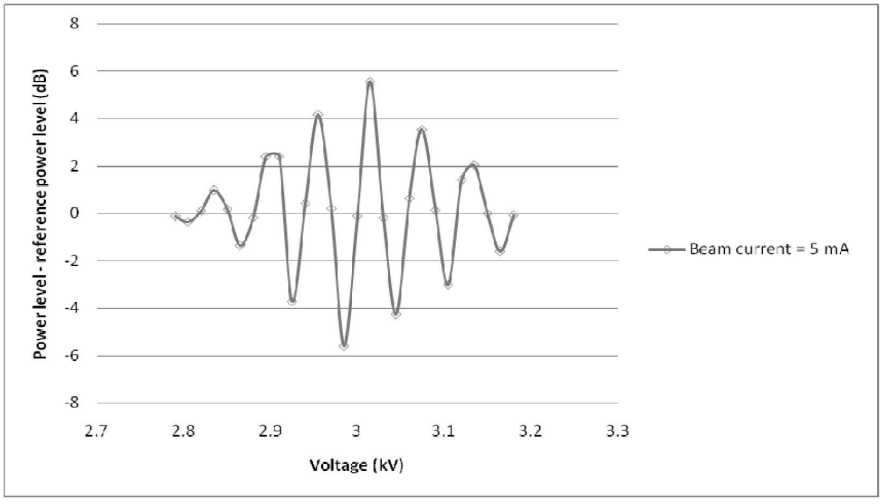

Figure 14. Gain-voltage curve for beam current of 5 mA.

obtained shows an interference pattern or oscillating characteristic and is deduced to be caused by the electron bunches moving successively in and out of phase with the EM wave as the beam voltage is varied. As the beam voltage is varied, so is the electron velocity. The maximum positive change in power, at 3.015 kV, is equal to a gain of 5.56 dB. As can be seen in Figure 9, the gain fluctuates depending on the accelerating voltage applied due to the bunching of electrons.

These results show that the low power PFEM prototype is producing gain which varies, in the correct manner with the beam voltage. The theoretical output power is 45 mWatt (16.56 dBm) if the usual parameters are used [1]. The obtained experimental result is 36 mWatt (15.5 dBm). The experimental result is approximately 20% less than the expected theoretical result. This is believed to be caused by the imperfection in the cavity construction, which causes losses. The copper mesh was constructed at a later stage, and this caused imperfection to the cavity especially near the mesh and aperture areas. At the X-band frequency of 10 GHz, the skin depth, δ, for the copper waveguide wall is 0.66×10^{-6} m, which is extremely small. Irregularities in the surface of the waveguide (in terms of solder material applied to the edges) could increase the loss of the waveguide.

A 360 degree phase shifter is placed at the output cavity, and this can be adjusted to ensure the correct phase between the bunched electron beams the microwave E-field in the output cavity. These bunched beams strongly interact with the microwave E-field in the output cavity. The plot of the power level-reference power level (dB) against the phase (degree) at 3015 Volts, 2955 Volts and 3075 Volts with 5 mA beam currents is shown in Figure 15. This plot can also be called as the gain-phase curve.

The curve with squares represents the 3015 Volts and 5 mA beam current, the curve with triangles represents the 2955 Volts and 5 mA beam current, while the curve with diamonds represents the 3075 Volts and 5 mA beam current. As can be seen from this figure, the best gain among the three voltages is at 3015 Volts, followed by 2955 Volts, and the least gain is at 3075 Volts. The result indicates that the electrons are pre-bunched in the input cavity. The EM wave is either increased or decreased after interaction with the electron beams depending on the relative phase between the two. If the phase difference is zero, the EM wave is amplified; if the phase is 180 degree, the wave is attenuated; if the phase is 90 degree, the EM wave is not affected. A high value point on the gain-curve implies that the phase of the electrons in the input cavity is the same as the phase of the EM wave in the output cavity. A low value point on the gain curve implies that the electrons in the input cavity and the EM wave in the output cavity are out of

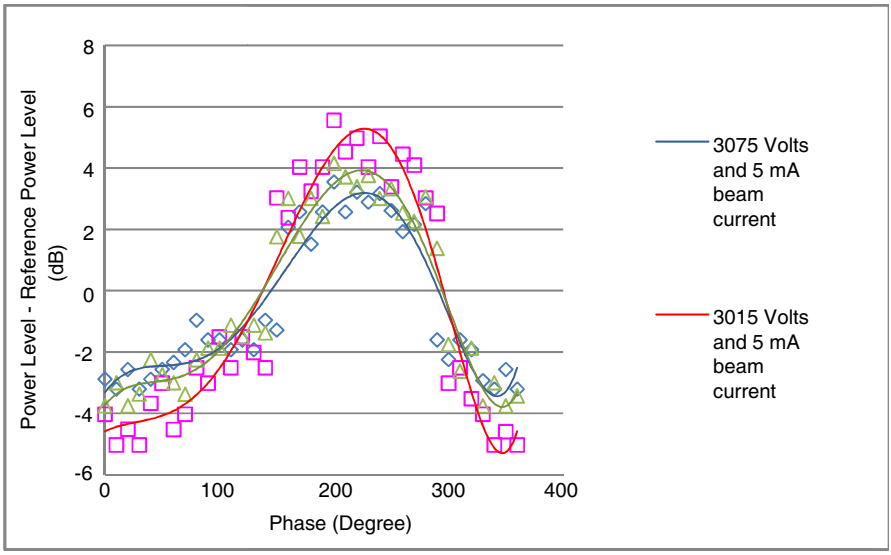

Figure 15. Comparison of gain-curves at 3015 Volts, 2955 Volts and 3075 Volts. All are using 5 mA beam currents.

phase.

The gain phase curves obtained are similar to the curve of the pre-bunched FEL total output power dependence on the phase delay between the bunching and FEL input fields, in the work done by Arbel et al. [25]. The power at the output cavity varies as the cosine of the phase angle of the electron beam as it enters the output cavity (to interact with the EM wave) [25]. The results obtained are consistent with the equation

$$P_2 = (00064)Q_2^2 Q_1 P_{1s} I^2 \cos(\Phi)$$

where P_2 is the output cavity (cavity power); Q_2 is the Q factor of the output cavity; Q_1 is the Q factor of the input cavity; P_{1s} is the seeding power; I is the beam current; Φ is the phase angle difference between the electron beam and EM wave in the output cavity.

6. CONCLUSION AND FUTURE WORK

Doria et al. have proposed a theory for the coherent emission and gain from a bunched electron beam passing through a waveguide FEM system [13]. Unfortunately, with a typical of 20 to 40 periods per wiggler, the length of the system would be large considering that the electron gun, accelerator and beam control would have to be

accommodated. A prototype low power PFEM has been built, which complies with many of the requirements defined for an FEL that is compact and low cost. Using available and affordable technology, a compact design (without wiggler) of the low power PFEM has been realized which uses a 3 kV, 5 mA electron beam, 10 mWatt seeded input power and X-band rectangular waveguide cavity. At this stage, the operating frequency used is 10 GHz. By incorporating the apertures in CONCERTO software, the leakage radiation of the E-field caused by the apertures has been analyzed. Various heights of the thin gap sections and apertures diameter have been simulated. These plots enabled us to calculate the electric field leakage (in Volts/mm) through the apertures.

After successfully producing a significant amount of current flowing across the apertures of the output cavity, the final experiment is performed by applying a high voltage in between the filament and input cavity. Thoria coated Iridium filament is used with a 5 mA beam current. Results obtained show that the highest gain is achieved at 3015 Volts with 5 mA beam current. The gain curve shows a bunching phenomenon of the electrons, where at different voltages, the gain varies sinusoidally. This shows that the electrons are in and out of phase from the EM wave depending on the voltage applied.

In the future, a 'Pierce' type electron gun could be proposed for the PFEM system. The 'Pierce' type electron gun could have a maximum emission current of 285 mA [26]. Hence, with the acceleration voltage of 3 kV, and the beam current of 142 mA (assuming 50% of the 285 mA current flow across the apertures of the output cavity), the resultant output power will be around 45 Watt. This value is derived from [1]. However, emission at higher beam currents will also mean that space-charge spreading of the beam must be taken into consideration [27].

The PFEM system can be scaled proportionately to operate at a higher frequency. For example, if the desired frequency is 20 GHz, the resulting height of the thin gap section would be 0.8 mm, while the acceleration voltage would still be maintained at 3 kV. Clearly, constructing the 0.8 mm height of the thin gap section would be complicated. Hence, another approach is to increase the acceleration voltage to 10.3 kV. This voltage is still considerably lower than previous FEL work at The University of Liverpool operating at 10 GHz. The voltage of 55.7 kV was used in [23], and around 70 kV was used in [26]. At higher frequencies, the use of waveguides to contain the radiation is no more practical. This is because of the very small waveguide dimensions, making construction really difficult and challenging. Therefore, the use of open resonators that propagates Gaussian beams should be investigated and considered [28, 29].

REFERENCES

1. Malek, F., J. Lucas, and Y. Huang, "Prototype design of compact and tuneable X-band pre-bunched free electron maser," *Progress In Electromagnetic Research*, PIER 85, 1–23, 2008.
2. Singh, G., "Analytical study of the interaction structure of vane-loaded gyro-travelling wave tube amplifier," *Progress In Electromagnetics Research B*, Vol. 4, 41–66, 2008.
3. Motz, H., "Applications of the radiation from fast electron beams," *J. Appl. Phys.*, Vol. 22, 527–535, 1951.
4. Sirkis, M. D. and P. D. Coleman, "The harmodotron — A megavolt electronics millimeter wave generator," *J. Appl. Phys.*, Vol. 28, 944–950, 1957.
5. Pantell, R. H., P D. Coleman, and R. C. Becker, "Dielectric slow-wave structures for the generation of power at millimeter and sub-millimeter wavelengths," *IRE Trans. Electron. Devices*, Vol. 5, 167–173, 1958.
6. Sjoberg, D., "Determination of propagation constants and material data from waveguide measurements," *Progress In Electromagnetics Research B*, Vol. 12, 163–182, 2009.
7. Dwari, S., A. Chakraborty, and S. Sanyal, "Analysis of linear tapered waveguide by two approaches," *Progress In Electromagnetics Research*, PIER 64, 219–238, 2006.
8. Mondal, M. and A. Chakrabarty, "Resonant length calculation and radiation pattern synthesis of longitudinal slot antenna in rectangular waveguide," *Progress In Electromagnetics Research Letters*, Vol. 3, 187–195, 2008.
9. De, A. and G. V. Attimarad, "Numerical analysis of two dimensional tapered dielectric waveguide," *Progress In Electromagnetics Research*, PIER 44, 131–142, 2004.
10. Lotfi Neyestanak, A. A. and D. Oloumi, "Waveguide band pass filter with identical tapered posts," *Journal of Electromagnetic Waves and Applications*, Vol. 22, No. 17–18, 2475–2484, 2008.
11. Panda, D. K. K., A. Chakraborty, and S. R. Choudhury, "Analysis of co-channel interference at waveguide joints using multiple cavity modeling technique," *Progress In Electromagnetics Research Letters*, Vol. 4, 91–98, 2008.
12. Hammou, D., E. Moldovan, and S. O. Tatu, "V-band microstrip to standard rectangular waveguide transition using a substrate integrated waveguide," *Journal of Electromagnetic Waves and Applications*, Vol. 23, No. 2–3, 221–230, 2009.

13. Doria, A., G. P. Gallerano, E. Giovenale, S. Letardi, G. Messina, and C. Ronsivalle, "Enhancement of coherent emission by energy-phase correlation in a bunched electron beam," *Physical Review Letters*, Vol. 80, No. 13, 2841–2844, March 30, 1998.
14. Pinhasi, Y. and Y. Lurie, "Generalized theory and simulation of spontaneous and super-radiant emissions in electronic devices and free-electron lasers," *Phys. Rev. E*, Vol. 65, 026501-1–8, 2002.
15. Doria, A., R. Bartolini, J. Feinstein, G. P. Gallerano, and R. H. Pantell, "Coherent emission and gain from a bunched electron beam," *IEEE J. Quantum Electron.*, Vol. 29, 1428–1436, 1993.
16. Oka, S., H. Togo, N. Kukutsu, and T. Nagatsuma, "Latest trends in millimeter-wave imaging technology," *Progress In Electromagnetics Research Letters*, Vol. 1, 197–204, 2008.
17. Ku, H. S.-L. and T. Yusaf, "Processing of composites using variable and fixed frequency microwave facilities," *Progress In Electromagnetics Research B*, Vol. 5, 185–205, 2008.
18. Mizuno, M., C. Otani, K. Kawase, Y. Kurihara, K. Shindo, Y. Ogawa, and H. Matsuki, "Monitoring the frozen state of freezing media by using millimetre waves," *Journal of Electromagnetic Waves and Applications*, Vol. 20, No. 3, 341–349, 2006.
19. Talaat Ibrahim, A., "Using microwave energy to treat tumors," *Progress In Electromagnetics Research B*, Vol. 1, 1–27, 2008.
20. Tiwari, K. C., D. Singh, and M. K. Arora, "Development of a model for detection and estimation of depth of shallow buried non-metallic landmine at microwave X-band frequency," *Progress In Electromagnetics Research*, PIER 79, 225–250, 2008.
21. Moradi, G., A. Ghorbani, M. Rahdan, and H. Khadem, "Analysis of output power delay in coaxial vircator," *Progress In Electromagnetics Research B*, Vol. 4, 1–12, 2008.
22. Topa, A. L., C. R. Paiva, and A. M. Barbosa, "Guidance and leakage behaviour of uniaxial ridge waveguides," *Journal of Electromagnetic Waves and Applications*, Vol. 23, No. 13, 1675–1684, 2009.
23. Dearden, G., "The industrial free electron laser," Ph.D. Thesis, Department of Electrical Engineering and Electronics, The University of Liverpool, U.K., 1993.
24. Oatley, C. W., "The tungsten filament gun in the scanning electron microscope," *Journal of Physics E: Scientific Instruments*, Vol. 8, 1037–1041, 1975.

25. Arbel, M., A. Abramovich, A. L. Eichenbaum, A. Gover, H. Kleinman, Y. Pinhasi, and I. M. Yakover, "Superradiant and stimulated superradiant emission in a prebunched beam free-electron laser," *Phys. Rev. Lett.*, Vol. 86, 2561–2564, 2001.
26. Wright, C. C., "Development of a free electron maser for industrial applications," Ph.D. Thesis, Department of Electrical Engineering and Electronics, The University of Liverpool, U.K., 2000.
27. Schiler, S., U. Heisig, and S. Panzer, *Electron Beam Technology*, Series 1, John Wiley & Sons, Inc., 1982.
28. Someda, C. G., *Electromagnetic Waves*, Series 1, CRC Press, 1998.
29. Hain, S., T. Honage, and W. Koch, "On resonances in open systems," *J. Fluid. Mech.*, Vol. 506, 255–284, 2004.